Expanded View Figures

Figure EV1. EM data analyses.

A Processing scheme including an exemplary micrograph and a subset of selected 2D classes of RZZ.
B Fourier shell correlation (FSC) curves of a global (i.e., non-focused) non-uniform 3D refinement in cryoSPARC. The dashed line indicates the 0.143 FSC criterion that intersects the masked FSC curve at 3.94 Å.
C Local resolution plotted on the locally filtered reconstruction obtained by non-uniform refinement in a rainbow-colored gradient from blue (3.7 Å) to red (8.0 Å).
D Angular distribution displayed as colored bars.

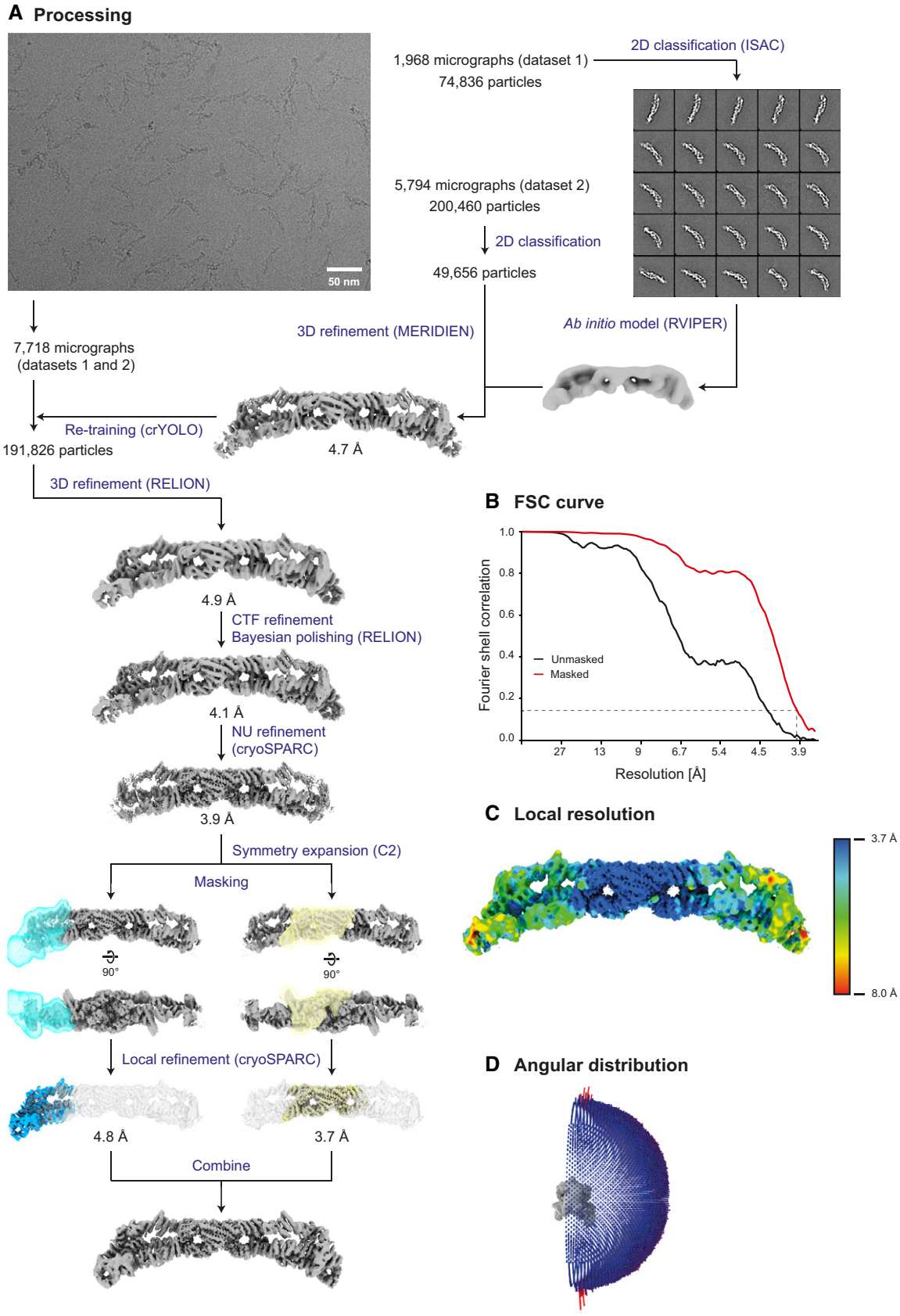

Figure EV1.

Figure EV2. Comparison between the HsROD and CeROD β-propellers.

A The farnesylated C-terminal tail of Spindly modeled on the AF2 ROD β-propeller. The side chains of Ile 589, Ser594, and Thr600 are predicted to point toward the ROD surface and were mutated to introduce a charge (Ile589Glu and Ser594Glu), and remove a potential for hydrogen bonding while rigidifying the main chain (Ser594Pro) and introducing a bulky group (Thr600Phe).

B Size-exclusion chromatography experiments with the indicated species demonstrating, to varying degrees, adverse effects of the mutations on assembly of RZZ–Spindly complex.

C The β-propeller of human ROD already shown in Fig 3B with the indicated farnesyl-binding site.

D β-propeller of *C. elegans*' ROD predicted by AlphaFold2 (Jumper *et al*, 2021; Tunyasuvunakool *et al*, 2021).

E, F Modeled farnesyl groups in the two structures based on predictions of the Spindly C-terminal peptide with AF2 demonstrate occlusion of the binding cavity in *C. elegans*, where M184 is predicted to sterically clash with a hypothetical farnesyl moiety.

Source data are available online for this figure.

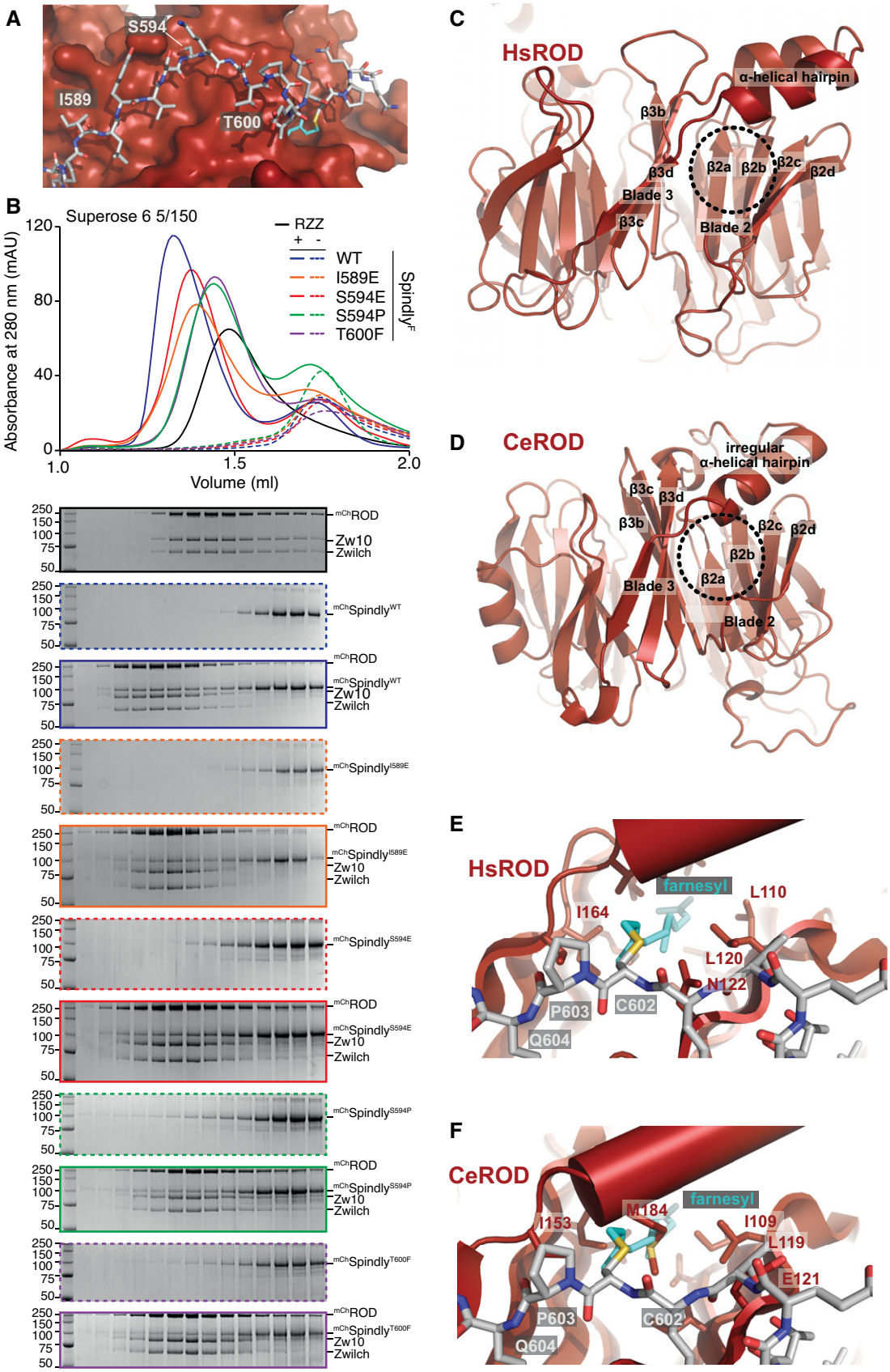

Figure EV2.

Figure EV3. Additional polymerization and cell biology experiments.

A Induced polymerization experiments with ^{mCh}RZZ, with or without wild-type Spindly^{F}, at the indicated temperatures. Several technical replicates were performed. Scale bar: 5 μm.

B, C Assessment of requirements for MPS1 phosphorylation for corona assembly *in vitro*. Samples 1–8 are shown on the left in Coomassie-stained and Pro-Q Diamond-stained SDS–PAGE. The content of samples 1–8 is described in the legend under panel B, and additionally for samples 2–5 over each polymerization experiment in panel C, where the encircled P signals which sample was pre-phosphorylated with MPS1 and which samples were treated with reversine to inhibit MPS1. In C, samples were imaged in a spinning disk confocal microscope at 561 nm. Scale bar = 5 μm. Two technical replicates were performed.

D Heat-induced polymerization experiments with ^{mCh}RZZ and wild-type Spindly^{F} or Spindly^{C602A} that cannot be farnesylated. The same positive control is also shown in Appendix Fig S3A. Two technical replicates were performed. Scale bar: 5 μm.

E Levels of BUB1 at kinetochores of HeLa cells that had been previously synchronized in G2 phase with 9 μM RO3306 for 16 h and then released into mitosis. Subsequently, cells were immediately treated with 500 nM reversine, 3.3 μM nocodazole, and 10 μM MG132 for 1 h. CREST serum was used to visualize kinetochores and DAPI to stain DNA. Scale bar: 10 μm. Three biological replicates were performed

F Scatter dot plots representing normalized intensity ratios of BUB1 over CREST for individual kinetochores of cells from the experiment shown in panel C. Red lines indicate median with interquartile range. Statistical analysis was performed with a nonparametric *t*-test comparing two unpaired groups (Mann–Whitney test). Symbols indicate n.s.$P > 0.05$, $*P \leq 0.05$, $**P \leq 0.01$, $***P \leq 0.001$, and $****P \leq 0.000$.

G HeLa cells were treated with 1 μM nocodazole for 4 h to prevent microtubule depolymerization and allow maximal corona expansion followed by 20 min of RO3306 treatment before fixation and further processed for fluorescence microscopy. CREST serum was used to visualize kinetochores and DAPI to visualize DNA. Scale bar: 10 μm. Two biological replicates were performed.

H HeLa cells treated like in panel E were released from the G2 arrest into mitosis for 1 h in the presence of 3.3 μM nocodazole, 500 nM hesperadin, and 10 μM MG132, fixed, and further processed for fluorescence microscopy. Three biological replicates were performed.

I Quantification of the experiment in panel H. Scatter dot plots represent normalized intensity ratios of the indicated proteins over CREST for individual kinetochores. Red lines indicate median with interquartile range. Statistical analysis was performed with a nonparametric *t*-test comparing two unpaired groups (Mann–Whitney test). Symbols indicate n.s.$P > 0.05$, $*P \leq 0.05$, $**P \leq 0.01$, $***P \leq 0.001$, and $****P \leq 0.000$.

Source data are available online for this figure.

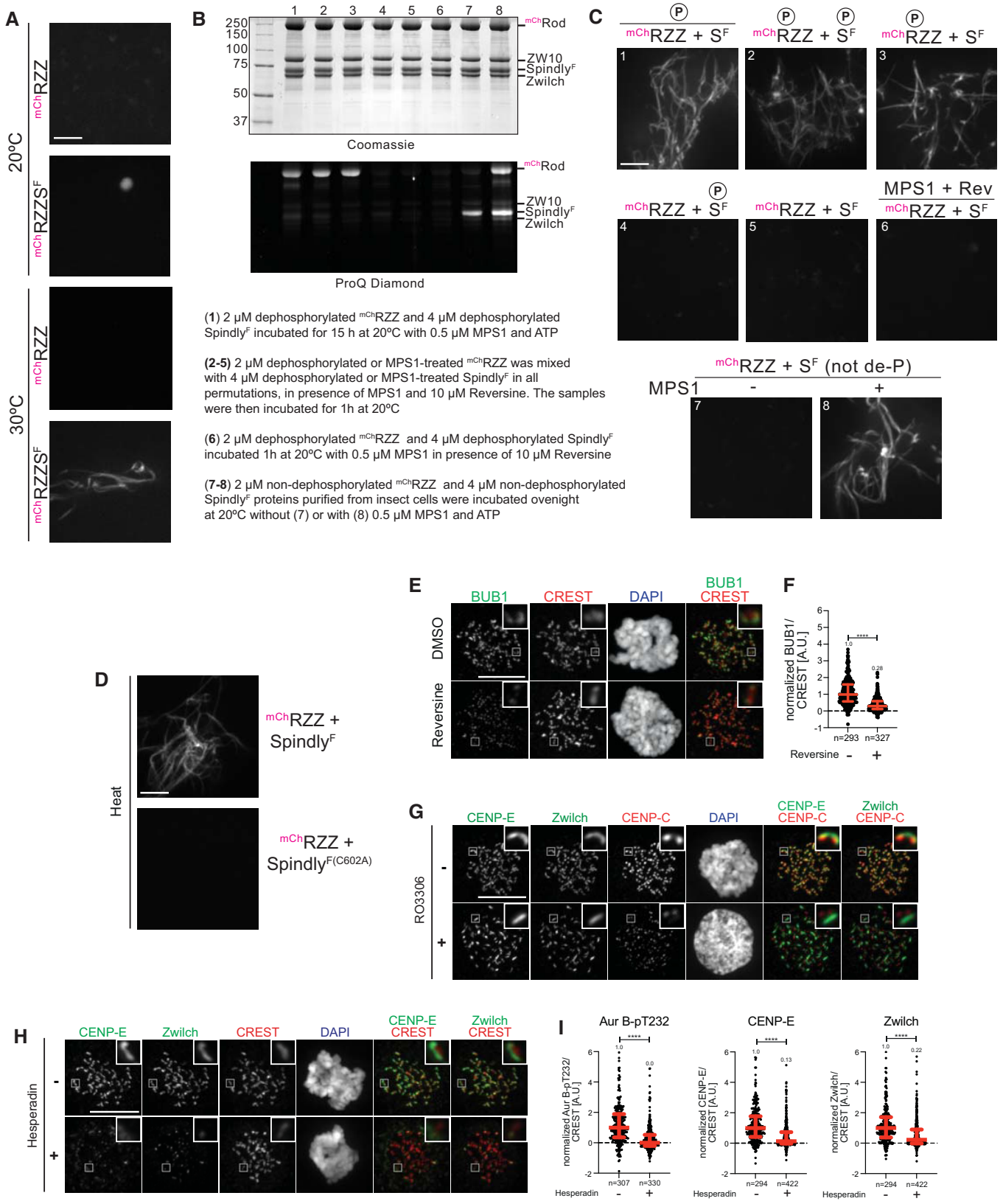

Figure EV3.

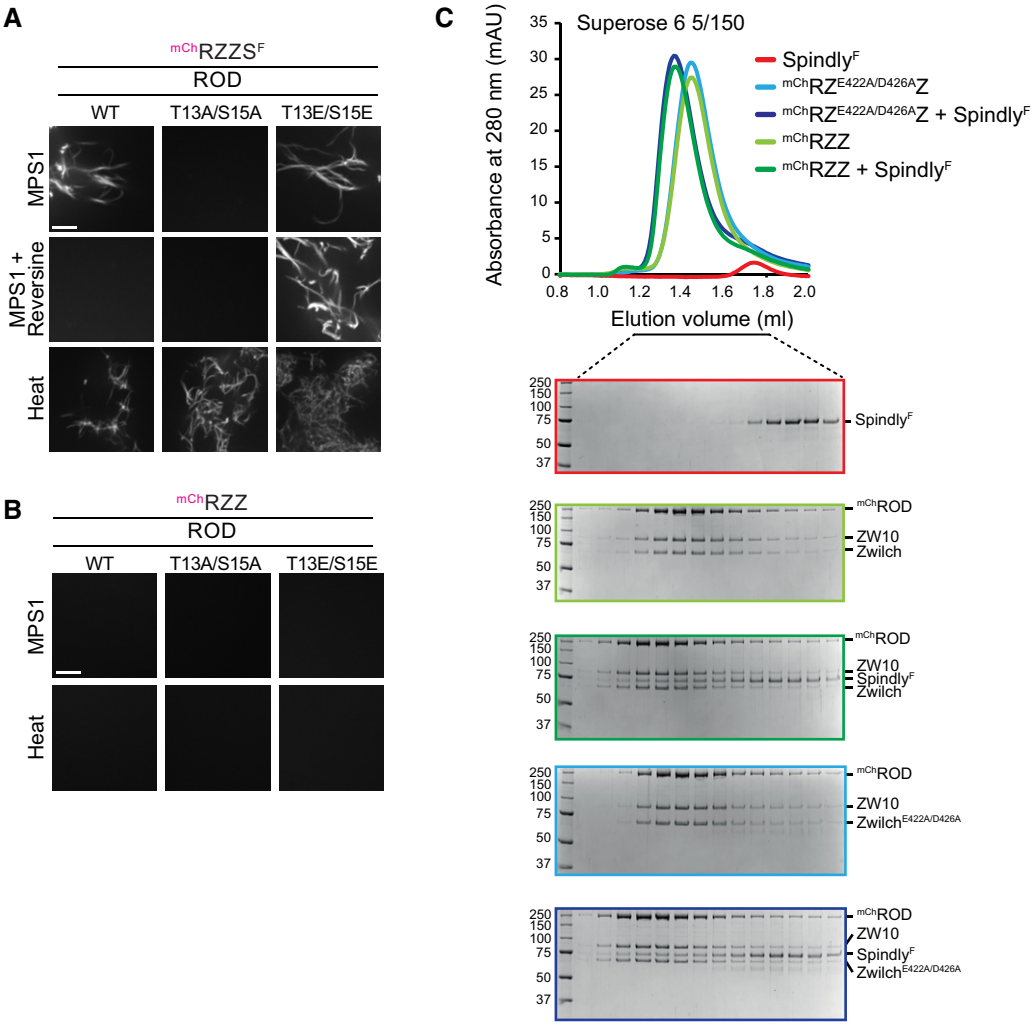

Figure EV4. Additional in vitro polymerization and biochemical experiments.

A The first two rows of experiments are already displayed as the two rows of Fig 5C The third row is added to demonstrate that the ^{mCh}RZZS^{F} complex carrying T13A/S15A mutations on ROD, which does not spontaneously filament in the presence of MPS1 at 20°C, will form filaments upon mild heating at 30°C, indicating that its ability to polymerize is not compromised. Scale bar: 5 μm.

B None of the indicated samples forms filaments in the absence of Spindly^{F}. Scale bar: 5 μm.

C Size-exclusion chromatography experiment demonstrating that RZZ complex carrying E422A/D426A mutations interacts with Spindly^{F} as strongly as its wild-type counterpart.

Data information: Experiments in panels A-B were technically replicated two times.
Source data are available online for this figure.

Figure EV5. Additional EM structural analyses.

A Untagged RZZS^{F} formed sheets indistinguishable from those formed by ^{mCh}RZZS^{F}. Scale bar (black line): 200 nm. Experiments were technically replicated at least three times.

B Sheets were also formed by ^{mCh}RZZS^{F} containing the T13A/S15A mutations on ROD upon heating the sample to 30°C. The phosphomimetic mutant T13E/S15E of the same complex assembled into filaments spontaneously at 20°C. The $^{mCh\text{-}\Delta15}$RZZS^{F} forms sheets at 30°C. Scale bar (black line): 200 nm. Two technical replicates were carried out.

C ^{mCh}RZZ/^{GFP}S^{F} formed ring structures or curved filaments similar to those observed with ^{mCh}RZZ/^{mCh}S^{F}. Scale bar (black line): 200 nm. At least three technical replicates were carried out.

D A size comparison from a field of ^{mCh}RZZ^{mCh}S^{F} filaments and the fluorescence signal of CENP-E at kinetochore coronas of nocodazole-treated HeLa cells is shown at the same magnification to emphasize the similarity of curvatures in rings and coronas. At least three technical replicates were performed.

E 2D class averages of segments of negatively stained single circles or filaments like those shown in panel C. Note the extreme orientation preference of the various classes. Scale bar: 50 nm.

F Representative micrograph of ^{mCh}RZZ/^{mCh}S^{F} rings in ice.

G Enlargement of one class average shown in panel E with indicated dimenssions.

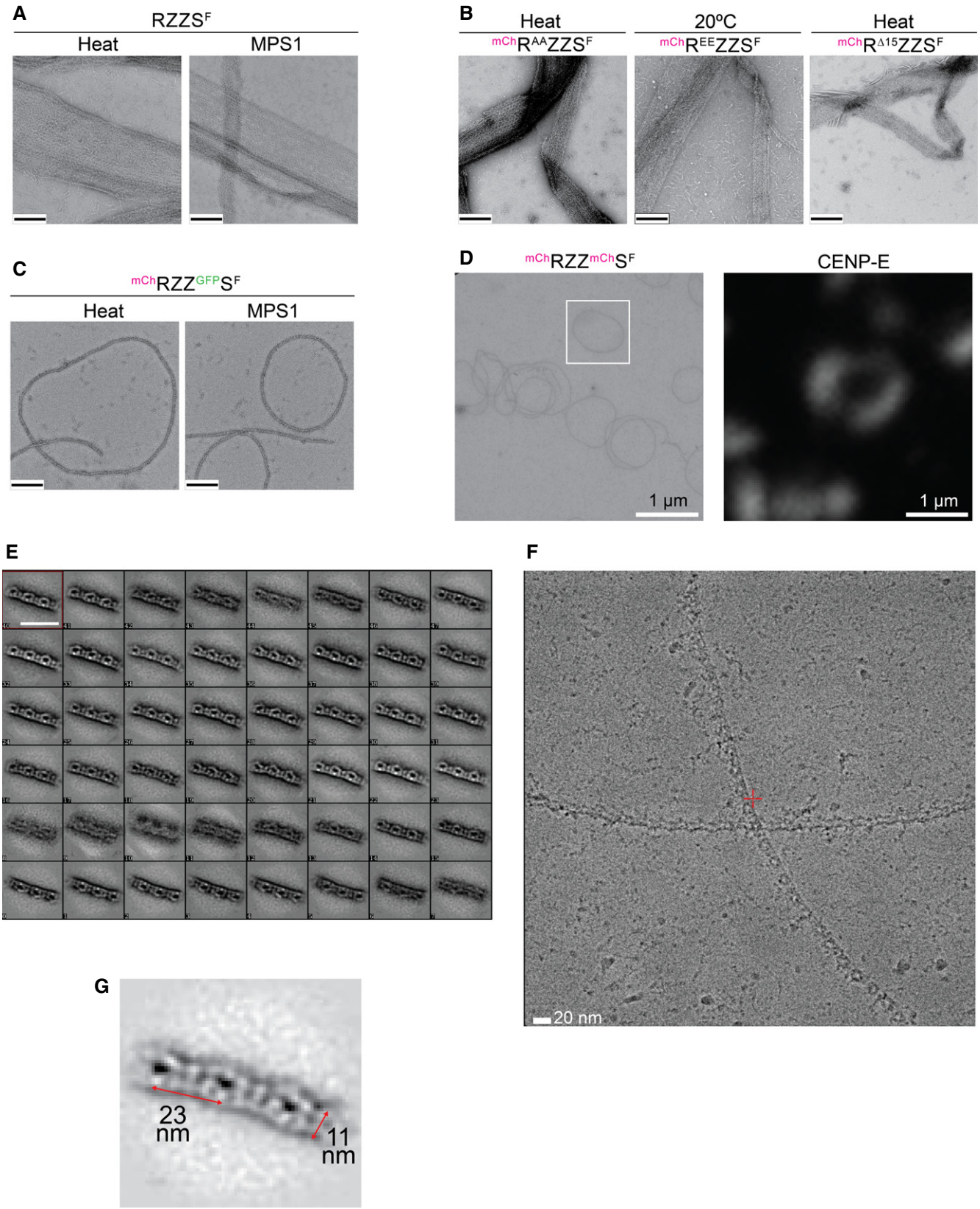
A
RZZS^{F}
Heat
MPS1
B
Heat
mChR^{AA}ZZS^{F}
20ºC
mChR^{EE}ZZS^{F}
Heat
mChR^{Δ15}ZZS^{F}
C
mChRZZ^{GFP}S^{F}
Heat
MPS1
D
mChRZZ^{mCh}S^{F}
1 µm
CENP-E
1 µm
E
F
20 nm
G
23 nm
11 nm

Figure EV5.